SEISMIC VULNERABILITY AND RESILIENCE OF LARGE-SCALE TELECOMMUNICATION NETWORKS

SEISMIC VULNERABILITY AND RESILIENCE OF LARGE-SCALE TELECOMMUNICATION NETWORKS

A. Cardoni[1], R. Tarantini[2], A. Calidori[2] & G. P. Cimellaro[2]

[1] Politecnico di Torino, Corso Duca degli Abruzzi 24, 10129 Turin, Italy, alessandro.cardoni@polito.it

[2] Politecnico di Torino, Corso Duca degli Abruzzi 24, 10129 Turin, Italy

Abstract: *Telecommunication networks play a key role in the economy of urban communities. As these infrastructures expand to meet the service demand, it is necessary to evaluate their vulnerability and resilience. Earthquakes and extreme natural events may cause severe damages to telecommunication towers which require multiple days of repair time. Despite some vulnerability studies have been carried out for tall raw-land towers and specific tower designs, large scale models at the network level are still lacking. In this paper, some of the most common rooftop tower designs are analyzed. Data is based on the city of Turin, Italy, and integrated in the telecommunication network of a virtual urban environment. Simplified structural models have been developed to describe the dynamic behavior of the rooftop towers. The input seismic action is represented by the acceleration time history at the top of each building. Consequently, the damage to the components mounted on the towers has been estimated based on the maximum displacement. Information about the failed components has been used to update the model of the network and to define vulnerability indexes that can be used in resilience analyses.*

1 Introduction

Telecommunication networks stand as indispensable infrastructures for urban communities, playing a pivotal role in both routine activities and critical situations like earthquakes. Over time, advancements in the design and seismic resilience of telecommunication infrastructure have emerged, inspired by a deeper understanding gained from the analysis of past earthquake impacts.

The existing body of literature addressing the vulnerability of such networks is relatively sparse. Few studies address the vulnerability assessment of telecommunication towers on a large scale. Most research focuses on the structural analysis of tall raw-land towers subjected to seismic actions and strong winds. Within the HAZUS methodology, FEMA has contributed seismic fragility curves for telecommunication facilities, outlining different damage states (FEMA (2003)). In the aftermath of the 2011 Great East Japan earthquake, Nemoto and Hamaguchi (2014) explored strategies aimed at enhancing the robustness of wireless networks. Their recommendations included swift recovery through mobile equipment, the establishment of an information distribution platform for data collection and decision-making, and the implementation of a mesh network fostering communication among satellites and unmanned aerial vehicles.

Another notable study by Gomes et al. (2016) delved into approaches for bolstering the robustness and resilience of communication systems in the face of natural disasters. They underscored that despite progress, the incidence of failures remains disproportionately high compared to other infrastructures, primarily

attributable to suboptimal design. In the broader context, there remains a notable gap in comprehensive methods for quantifying vulnerability and resilience on a large scale.

This paper proposed a physical-based procedure for a preliminary vulnerability analysis of urban telecommunication networks. The case study is the *Ideal City* virtual environment, which is inspired by the city of Turin, Italy (Marasco et al. (2020)). The network was modeled through a crowdsourced database and satellite imagery inspection. To define the connectivity among the base station controllers (BSCs) a hierarchical three-layer topology was chosen, while base station transceivers (BTSs) were connected to BSCs according to a star scheme. The performance of the infrastructure was assessed in terms of throughput under a simulated seismic scenario. Two metrics were proposed to assess the networks' performance. The first one is based on the physical damage to the towers, while the second on the performance in terms of throughput.

2 Telecommunication network model

2.1 Topology of the network

Modeling the network often represents a challenge itself, as in most cases the infrastructure is privately owned, and companies are unwilling to share their data. This poses a serious limitation for researchers to carry on analyses at a large scale. In this work we overcome the problem using a combination of public data sources. The majority of information to model the network was retrieved from the website CellMapper, which is a crowd-sourced database for cellular tower and coverage mapping (CellMapper (2021)). The case study used to implement and test the methodology is a virtual testbed called *Ideal City*. It is inspired by the city of Turin in Italy, representative of a typical medium sized European city. Through CellMapper it was possible to obtain coordinates of antennas, frequency bands, bandwidth, mobile network operators (MNOs). The GIS map of Turin (Geoportale (2021)) and satellite imagery from Google Maps (Google (2021)) were also consulted to verify and extend the data collection.

The main elements of wireless telecommunication networks at the urban level are: (1) base station controllers (BSCs); (2) base transceiver stations (BTSs), i.e. steel structures where antennas are mounted and a technical compartment with electronic devices located nearby; (3) user equipment (UE), i.e., mobile devices.

The visual inspection of satellite imagery was crucial to distinguish BSCs from BTSs. At the end of the data collection phase 387 BTSs and 18 BSCs were identified, which are reasonable numbers for a city of about 900,000 people and given that each BSC usually controls between 10 and 20 BTSs (Giovinazzi et al. (2017)). This effort was also essential to estimate the structure type and height of the antenna towers. In the urban area, the physical infrastructure is owned and operated by three MNOs. In this work, the network owned by MNO_2, which serves the 32.9% of the population, is considered.

The generated database also contains information about cell types and transmission frequencies. Macro cells are characterized by an 800 MHz frequency (band 3) while micro cells by an 1,800 MHz frequency (band 20).

Figure 1 shows the spatial distribution of BSCs, raw-land and rooftop BTSs, and some features of the network.

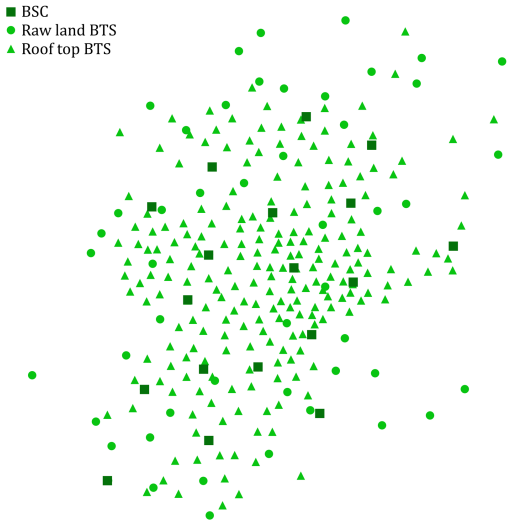

	MNO_2
No. of BTS	359
No. of Towers	286
No. of Raw land towers	53
No. of Rooftop towers	233
No. of Raw land macro cells	25
No. of Raw land micro cells	46
No. of Rooftop macro cells	83
No. of Rooftop micro cells	205
Raw land towers height	25 – 45m
Rooftop towers height	2 – 6m
No. of Raw land posts	33
No. of Raw land masts	20
No. of Rooftop posts	170
No. of Rooftop masts	63
Customer share	32.9%

Figure 1: Elements and characteristics of the network.

The next challenge faced was determining the way the physical elements of the network were connected as this is also another confidential information belonging to infrastructure owners. Based on common infrastructure designs, a hybrid topology was adopted considering that:

1. BTSs are connected to BSCs through a star topology. The primary criterion employed for establishing connections was the selection of the shortest distance, with the underlying assumption being that all connections would be implemented through underground cables. This particular topology offers several advantages. Firstly, in the event of a BTS node failure, the remainder of the network remains operational. Secondly, the system's scalability is enhanced, allowing for straightforward expansion through the addition of more connections and nodes. Thirdly, the topology facilitates efficient and robust data transfer. However, it is crucial to acknowledge certain drawbacks, including potential cost implications arising from the length of connections and the vulnerability of a BSC failure causing a cascade effect, leading to the failure of all BTSs downstream.
2. To further elaborate on the structure, the BSCs were organized in a hierarchical three-layered arrangement, resembling a fat tree. This proposed topology comprises two core nodes, each intricately linked to four aggregation nodes. Each aggregation node, in turn, establishes six connections to the edge nodes, ensuring that each edge node maintains connectivity with two distinct aggregation nodes. The classification of BSCs into core, aggregation, and edge nodes was based on geographic location and facility size. Internal BSCs were designated as core nodes, followed by the nearest ones as aggregation nodes, with the remaining nodes categorized as edge nodes. Figure 2 provides a visual representation of MNO_2 network's topology.

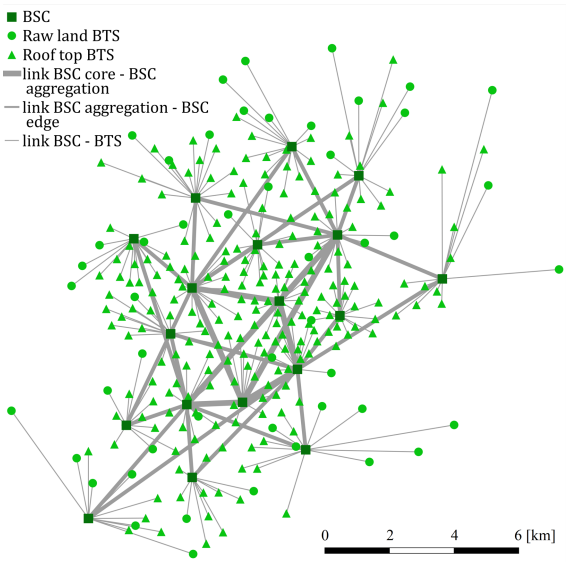

Figure 2: Topology of the MNO_2 network.

2.2 Characterization of rooftop telecommunication towers

The identified rooftop towers are either steel poles or masts with varying height as indicated in Figure 1. Getting data regarding the section dimensions, connection type, year of installation is particularly challenging at the urban scale. Therefore, a simplified procedure was followed to design the sections. In this analysis, the procedure and results obtained for the pole-type structures are shown. The steel members were considered as cantilever beams with a fixed connection at the base. They were grouped into nine categories based on their height, which varies from 2.5 m to 6.0 m with steps of 0.5 m. It was assumed they are all made of steel S275 J0 and have a circular hollow section. To design the section, considering the limited heights and loads, the following slenderness formula was used: $\lambda = l_0/\rho$, where λ is the slenderness, ρ is the radius of gyration, $l_0 = 2 \cdot l$ considering that the pole length is equal to l. Table 1 describes the main parameters of the nine section categories, identified by their values of diameter (D) and thickness (t) in mm.

Table 1: Characteristics of pole structures.

Section category	Height [m]	Area [cm^2]	Moment of inertia [cm^4]	Radius of gyration [cm]	Linear weight [kg/m]
D 60.3 t 3.2	2.0	5.74	23.47	2.02	4.51
D 76.1 t 5	2.5	11.17	70.92	2.52	8.77
D 88.9 t 4	3.0	10.67	96.34	3.00	8.38
D 114.3 t 10	3.5	32.77	449.66	3.70	25.72
D 139.7 t 12.5	4.0	49.95	1020.01	4.52	39.21
D 139.7 t 12.5	4.5	49.95	1020.01	4.52	39.21
D 168.3 t 12.5	5.0	61.18	1868.35	5.53	48.03
D 168.3 t 12.5	5.5	61.18	1868.35	5.53	48.03
D 193.7 t 16	6.0	89.32	3554.26	6.31	70.12

A finite element model of each beam was developed. The beams were discretized into 25 elements and the relative masses were applied at each node. Three antennas are supposed to be installed at the top of each element, for a total lumped load of 0,75kN. Only the flexural stiffness was taken into account.

3 Vulnerability assessment

3.1 Vulnerability of the network

Within the existing scientific literature, there is a notable scarcity of studies pertaining the vulnerability of telecommunication network at the urban level. Commonly, antennas are installed on steel structures such as masts and monopoles. While FEMA (2003) has supplied fragility curves for telecommunication facilities, a noticeable gap exists in the research concerning the seismic vulnerability of the towers themselves, particularly

those that are roof mounted. The inherently private management of these networks, coupled with the confidentiality of data, presents a substantial challenge in conducting detailed seismic damage simulations. The constraints imposed by data confidentiality makes it difficult to execute comprehensive analyses, necessitating numerous assumptions regarding section dimensions, types of elements, and the nature of connections. Additionally, despite the robust design of towers that sometimes allow them to withstand even strong ground motions, vulnerabilities arise as cables and other electrical components are susceptible to damage when subjected to substantial displacements and rotations.

Firstly, the vulnerability of the towers is inherently linked to the vulnerability of the buildings on top of which they are located. Simply put, if a building collapses, the tower and BTS would inevitably fail in tandem. The methodology to estimate the building damage under a seismic scenario is described by Marasco et al. (2020). Overall, the advantage of having a virtual testbed is that it allows to apply any seismic scenario via a simplified procedure using epicenter location, moment magnitude, and the actual acceleration record or the event recorded at the epicenter. Then, at each building location, two horizontal seismic inputs are applied considering the principal axes of the building. The Ambraseys ground motion model was used to define each seismic input (Ambraseys et al. (1996)). After performing nonlinear time history analyses, the maximum inter-storey drift was calculated for each structure and linked to a structural damage state using the method introduced by Ghobarah (2004).

Then, to assess the damage to the towers and to the electronic components, the acceleration time histories computed at the top of each building along the two horizontal principal directions were used as input at the base of each tower. The accelerations were calculated following the procedure introduced in (Marasco et al. (2020)). Thus, nonlinear dynamic analyses were conducted to compute the top displacement time histories. Based on the maximum top displacements drift ratios were calculated. According to the Structural Standard for Antenna Supporting Structures and Antennas and Small Wind Turbine Support Structures (TIA-222-H (2017)), a 3% drift ratio is sufficient to make the electronic components unserviceable.

3.2 Vulnerability metrics for resilience

To quantify the vulnerability of the network, two metrics were introduced. The first one refers to the robustness of the network, being defined as the ratio between the number of towers that remain functional after the earthquake (n) and the total number of towers (N_T).

$$R_{TOW} = \frac{n}{N_T} \tag{1}$$

When the value of R_{TOW} is close to 1, the network is robust. By this definition, this metric could also be seen as a descriptor of redundancy as redundant networks would most likely have a large value of R_{TOW}. Moreover, based on the post-event value of this metric, an economic loss due to repair, replacement, and downtime could be estimated, giving a valuable input to a detailed resilience analysis.

The second metric is related to the quality of service experienced by the users. It is defined by dividing the post- and pre-earthquake mean throughput:

$$R_{THR} = \frac{\overline{THR}_{post}}{\overline{THR}_{pre}} \tag{2}$$

Since Ideal City's population has been divided into clusters that represents the number of people resident in each building, $\overline{THR}$ is the throughput weighted by the number of users in each cluster:

$$\overline{THR} = \frac{\sum_{i=1}^{k} N_{U,i} \cdot THR_i}{N_U} \tag{3}$$

In Equation 4, $N_{U,i}$ is the cluster's number of users, k is the clusters number, THR_i is the best value of throughput for the *i-th* cluster, and N_U is the total number of users. When R_{THR} is low the users will experience

poor throughput meaning the network performance decreases. The next section provides more details about the performance assessment in terms of throughput.

4 Performance assessment

In this study the throughput, i.e., the rate of successfully delivered data per time unit (Miao et al. (2016)), was used to describe the network performance. By its definition, a higher throughput corresponds to a better quality of service for the users. At the base of it there is the calculation of the signal to interference plus noise ratio (SINR), which is defined as the ratio between the received signal power (P) and the sum of interference (I) and noise (N):

$$SINR = \frac{P}{I + N} \tag{4}$$

The received signal power is calculated as the difference between the transmission power (*PT*) and the path loss (*PL*). Based on common values, *PT* was assumed equal to 43 dBm for macro cells and 30 dBm for micro cells (Wannstrom (2013), ITU (2015)). On the other hand, to determine the path loss, the models proposed by the International Telecom Union (ITU) were assumed (ITU (2009)).

In the computation of interference, an assumption was made that the network operates with a frequency reuse factor set at 1. This assumption is conservative hypothesis that means that BTSs have the ability to utilize all frequencies at their disposal. Consequently, the chosen frequency reuse factor of 1 implies an exceptionally high level of interference, making the impact of noise (N) less relevant. For this reason, the calculation of noise was omitted.

Figure 3 shows the SINR for one user cluster with respect to all macro and micro cells.

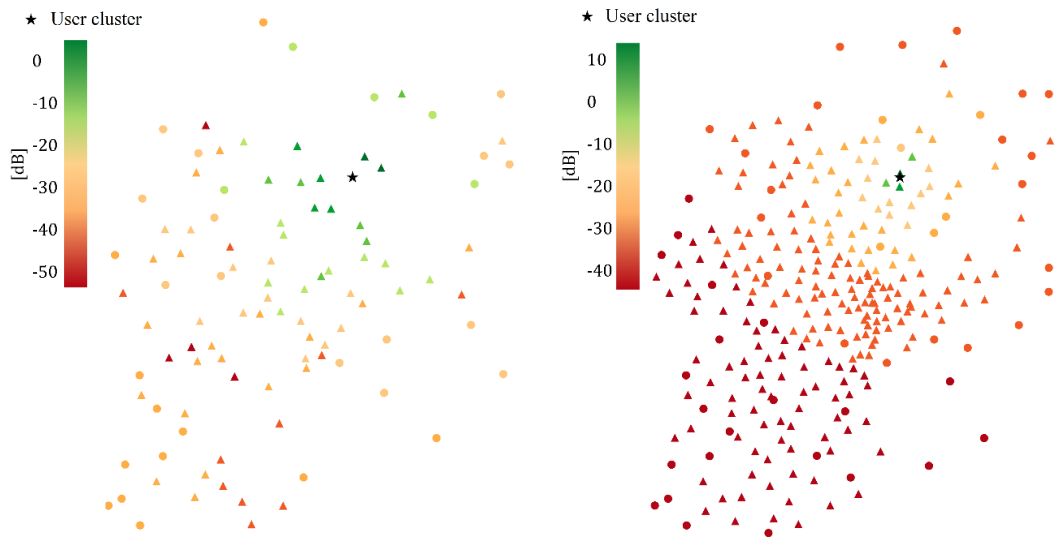

(a) (b)

Figure 3: Visual representation of the SINR for a user cluster considering (a) macro and (b) micro cells.

Each band is associated to a different channel bandwidth (BWs). Table 2 reports the summarizes characteristics of bands 3 and 20 based on the “E-UTRA Operating Bands” and “E-UTRA Channel Bandwidth” documentation (3GPP (2010)).

Table 2: Characteristics of bands 3 and 20.

Band	Duplex mode	Frequency [MHz]	Uplink [MHz]	Downlink [MHz]	Channel bandwidths [MHz]
3	FDD	1,800	1,710 - 1,785	1,805 - 1,880	1.4, 3, 5, 10, 15, 20
20	FDD	800	832 - 862	791 - 821	5, 10, 15, 20

To get the throughput from the SINR a mapping procedure was followed. The SINR-throughput relation depends on the modulation as reported by Olmos et al. (2010). In this research, a subset of 14 modulation coding schemes (MCSs) defined by the LTE standard for a BW of 10 MHz was considered, similarly to the procedure presented by Mühleisen, et al. (2011). The 10 MHz BW was assumed for both bands given the lack of better knowledge, which is a cautious hypothesis given the standards of modern networks. Under this hypothesis, there are 50 available resource blocks (RBs) for each BW. To ensure full capacity of uplink and downlink, the frequency division duplex mode was chosen. Based on the MCS the BTS selects the transport block size (TBS) (Fan et al. (2011)), which is then used to calculate the number of bits that can be transmitted (Rathi et al. (2014)). The data transmitted can be increased by using multiple antennas. In modern networks, it is common for the receiver and the transmitter to use a multiple-input-multiple-output (MIMO) configuration (Lee at al. (2009)). Thus, a 2x2 MIMO scheme was chosen. Thanks to this procedure it is possible to calculate the SINR-throughput functions. The linear envelop curve was then extracted (Figure 4). This represents the ideal situation where users get the best modulation. Although ideal, the use of this curve is somewhat justified by the fact that a frequency reuse factor equal to 1 that generates large interference was used.

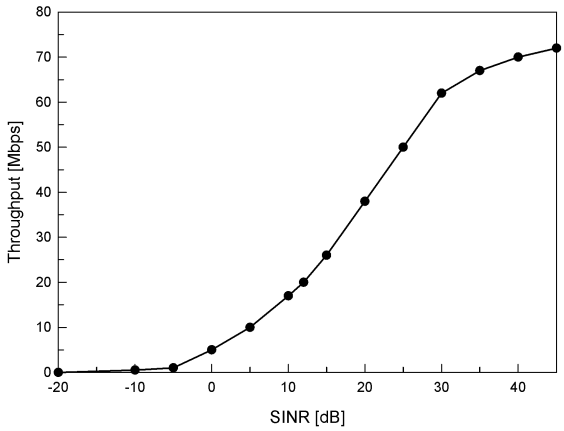

Figure 4: Mapping envelope curve between SINR and throughput.

5 Case study

The proposed procedure was tested on Ideal City under the 2016 Central Italy earthquake (date: 10/30/2016, M_w = 6.5, depth = 9 km, peak ground acceleration = 0.3 g). Based on the results of the building damage assessment, the collapsed buildings hosting BTSs and BSCs were identified. Figure 5 shows the damage map after the earthquake. The map allows for a preliminary and straightforward understanding of the impact of the event. The collapse of BSCs was a key factor. Under the applied scenario, the actual number of collapsed towers because of the building collapse was only 14, but since 2 out of 18 BSCs collapsed, the total number of failed towers increased to 89 (Figure 6).

The nonlinear time history analysis on the rooftop towers revealed that the steel poles reported no structural damage, staying abundantly within the elastic domain. The maximum top displacements of the steel members ranged between 10 and 40 mm and the resultant drift was consistently lower than the 3% drift limit, ranging between about 0.3 and 1.8%. Consequently, it can be stated that none of the electronic devices get damaged and the BTSs are still functional. Therefore, considering the proper vulnerability of the steel structure did not modify the results. It is worth noticing that considering the mast towers would have led to even lower drift ratios given the stiffer nature of such section design. The R_{TOW} index is equal to 0.69 indicating a good robustness of the network.

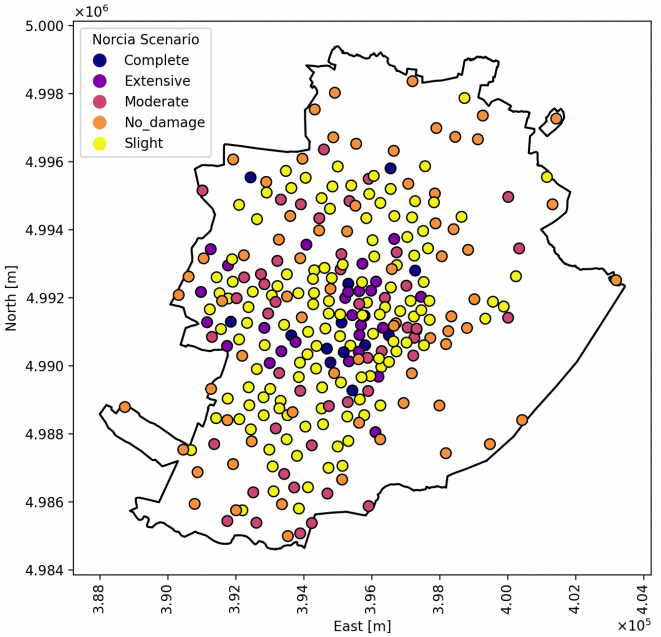

Figure 5: Damage suffered by the buildings hosting BTSs and BSCs after the seismic scenario.

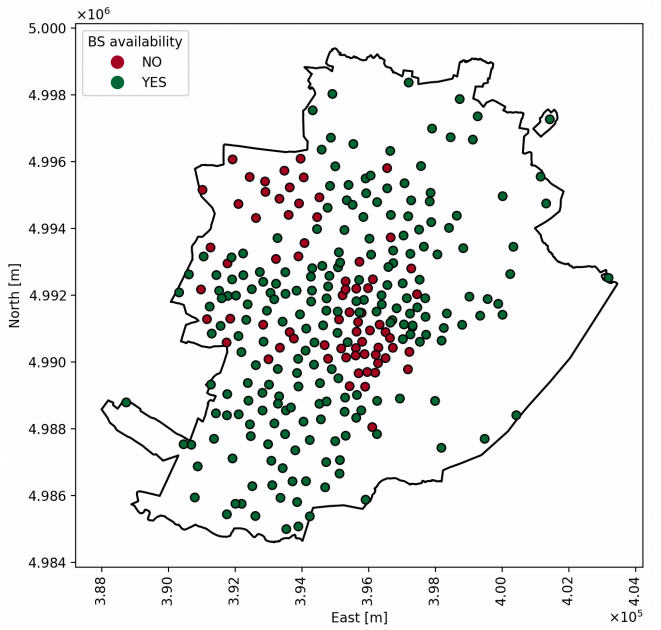

Figure 6: Failed BTSs and BSCs after the seismic scenario.

Once failed towers were identified and removed from the network model, a post-event throughput was calculated for each cluster. Figure 7 shows the most critical part of the throughput map in normal conditions and after the earthquake. As expected, the throughput tends to decrease. However, it was observed that users closer to functional BTSs might benefit from a better performance because the interference decreases. The mean weighted throughput in normal conditions was $\overline{THR}_{pre}$ = 20.14 Mbps, while the vulnerability index was R_{THR} = 0.9 indicating a slight yet significant reduction in the quality of service.

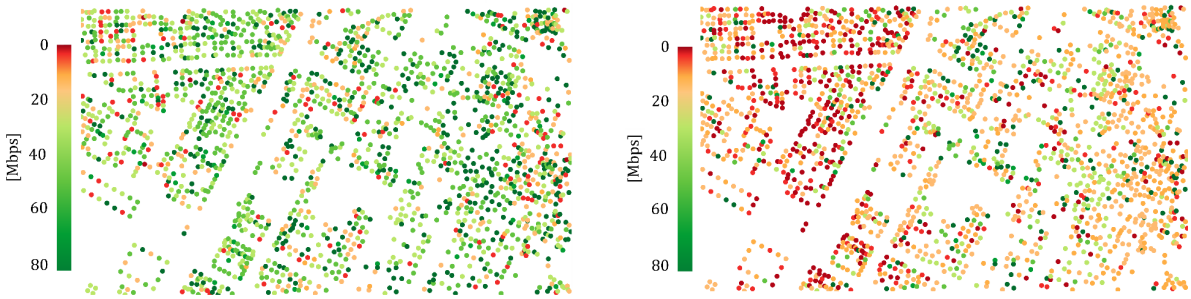

(a) (b)

Figure 7: Throughput in (a) normal conditions and (b) after the seismic scenario.

6 Conclusions

This study aimed to assess the seismic vulnerability of telecommunication networks, focusing on the physical infrastructures owned and managed by an MNO. The modeling process involved leveraging information sourced from a crowdsourced website and satellite imagery. To establish connectivity, a hybrid topology scheme was implemented, utilizing a three-layer fat tree hierarchy approach.

To gauge the network's performance under a simplified seismic scenario, two vulnerability metrics were introduced. The first metric reflects the vulnerability of the towers, serving as a proxy for robustness and economic loss. The second metric evaluates the network's performance and service quality in terms of data transfer, i.e., throughput.

It is important to note that this methodology is designed as a preliminary tool, and the outcomes are contingent on the chosen topology, potentially varying with an alternative topology scheme. Recognizing the large-scale nature of the problem and the scarcity of detailed information, certain simplifications were unavoidable. Notably, the vulnerability of the telecommunication network resulted to be solely connected to the building damage, as the towers' drift ratios were far below the threshold to observe damage in the electronic components. This implies that further research is needed to include detailed design conditions such as connection type and ageing of the materials.

Moreover, since comprehensive data on network traffic was unavailable, assumptions had to be made regarding user connections. The research operated on the hypothesis that all users connect simultaneously, representing the most unfavorable scenario. Despite these simplifications, the presented procedure can yield valid results, serving as a foundational framework for evaluating the seismic resilience of urban telecommunication networks.

7 References

3GPP, "Further advancements for E‐UTRA physical layer aspects," 3GPP TR 36.814, Tech. Rep, 2010.

N. N. Ambraseys, K. u. Simpson, and J. J. Bommer, "Prediction of horizontal response spectra in Europe," Earthquake Engineering & Structural Dynamics, vol. 25, pp. 371-400, 1996.

CellMapper. (2021). Cellular Coverage and Tower Map. Available: https://www.cellmapper.net/

J. Fan, Q. Yin, G. Y. Li, B. Peng, and X. Zhu, "MCS selection for throughput improvement in downlink LTE systems," in 2011 Proceedings of 20th international conference on computer communications and networks (ICCCN), 2011, pp. 1-5.

FEMA, "Multi-hazard loss estimation methodology, earthquake model," Washington, DC, USA: Federal Emergency Management Agency, 2003.

Geoportale. (2021). Geoportale e governo del territorio. Available: https://geoportale.comune.torino.it/

A. Ghobarah, "On drift limits associated with different damage levels," in International workshop on performance-based seismic design, 2004.

S. Giovinazzi, A. Austin, R. Ruiter, C. Foster, M. Nayyerloo, N.-K. Nair, et al., "Resilience and fragility of the telecommunication network to seismic events," Bulletin of the New Zealand Society for Earthquake Engineering, vol. 50, pp. 318-328, 2017.

Google. (2021). Google Maps. Available: https://maps.google.com/

T. Gomes, J. Tapolcai, C. Esposito, D. Hutchison, F. Kuipers, J. Rak, et al., "A survey of strategies for communication networks to protect against large-scale natural disasters," in 2016 8th international workshop on resilient networks design and modeling (RNDM), 2016, pp. 11-22.

J. Lee, J.-K. Han, and J. Zhang, "MIMO technologies in 3GPP LTE and LTE-advanced," EURASIP Journal on wireless communications and networking, vol. 2009, pp. 1-10, 2009.

S. Marasco, A. Cardoni, A. Z. Noori, O. Kammouh, M. Domaneschi, and G. P. Cimellaro, "Integrated platform to assess seismic resilience at the community level," Sustainable Cities and Society, p. 102506, 2020.

G. Miao, J. Zander, K. W. Sung, and S. B. Slimane, Fundamentals of mobile data networks: Cambridge University Press, 2016.

M. Mühleisen, D. Bültmann, R. Schoenen, and B. Walke, "Analytical evaluation of an IMT-advanced compliant LTE system level simulator," in 17th European Wireless 2011-Sustainable Wireless Technologies, 2011, pp. 1-5.

Y. Nemoto and K. Hamaguchi, "Resilient ICT research based on lessons learned from the Great East Japan Earthquake," IEEE Communications Magazine, vol. 52, pp. 38-43, 2014.

J. Olmos, S. Ruiz, M. García-Lozano, and D. Martín-Sacristán, "Link abstraction models based on mutual information for LTE downlink," in COST, 2010, pp. 1-18.

S. Rathi, N. Malik, N. Chahal, and S. Malik, "Throughput for TDD and FDD 4 G LTE Systems," International Journal of Innovative Technology and Exploring Engineering (IJITEE), ISSN, pp. 2278-3075, 2014.

P. Series, "Propagation data and prediction methods for the planning of short-range outdoor radiocommunication systems and radio local area networks in the frequency range 300 MHz to 100 GHz," tech. rep., ITU, Tech. Rep. ITU-R, 2015.

M. Series, "Guidelines for evaluation of radio interface technologies for IMT-Advanced," Report ITU, vol. 638, pp. 1-72, 2009.

TIA-222-H Structural Standard for Antenna Supporting Structures and Antennas and Small Wind Turbine Support Structures. 2017

J. Wannstrom, "LTE-advanced," Third Generation Partnership Project (3GPP), 2013.